Materials and Design 189 (2020) 108525

Contents lists available at ScienceDirect

Materials and Design

journal homepage: www.elsevier.com/locate/matdes

Fabrication of ZnO@C foam: A flexible free-standing electrode for energy storage devices

Zohre Fahimi, Omran Moradlou *

Department of Chemistry, Faculty of Physics & Chemistry, Alzahra University, P.O. Box: 1993893973, Tehran, Iran

HIGHLIGHTS

- A flexible ZnO@C foam was fabricated as supercapacitor electrode/support.
- ZnO@C foam exhibits enhanced areal specific capacitance of 1120 mFcm^{-2} at 4 mA cm^{-2}.
- The foam provides improved charge transfer rate and high electrical conductivity.
- The asymmetric device delivers high energy density and excellent cycling stability.
- ZnO@C benefits high potential applicability in energy storage and production devices.

GRAPHICAL ABSTRACT

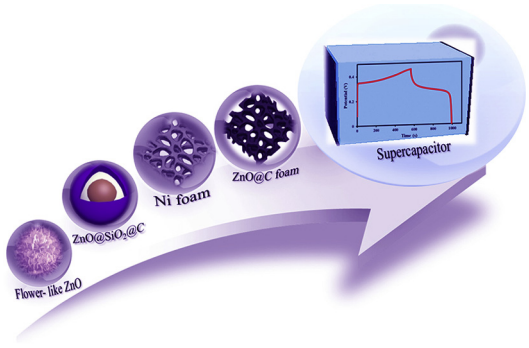

ARTICLE INFO

Article history:
Received 20 September 2019
Received in revised form 23 January 2020
Accepted 24 January 2020
Available online 25 January 2020

Keywords:
ZnO@C foam
Flexible
Energy storage devices
Supercapacitor

ABSTRACT

In this work, we have synthesized a flexible ZnO@C foam for its potential applications in energy production and storage devices based on the simple and versatile method. The fabricated ZnO@C foam exhibited enhanced capacitance compared to commercially available Ni foam. The fabrication process involves the synthesis of ZnO nanostructures, deposition of ZnO@C nanostructure on Ni foam, and finally, removing Ni substrate to have ZnO@C foam. Based on cyclic voltammetry, galvanostatic charge-discharge curves and electrochemical impedance spectroscopy, it was concluded that the ZnO@C foam has a suitable electron transfer rate and conductivity. ZnO@C foam provides a high areal specific capacitance of 1120 mF cm^{-2} at a current density of 4 mA cm^{-2}. The proposed flexible foam has potential applications in the fabrication of solid-state supercapacitors as well as fuel cells.

1. Introduction

Supercapacitors, batteries and fuel cells are upcoming technologies for clean energy storage and production [1]. In these techniques, the electrodes play an important role and make a major contribution to performance and cost of the device [2,3]. In supercapacitors as promising

* Corresponding author.
E-mail address: moradlou@alzahra.ac.ir (O. Moradlou).

https://doi.org/10.1016/j.matdes.2020.108525

energy storage devices [4,5], the required electrode characteristics are their low-cost, high specific surface area, high capacity, fast electron transfer rate and good electrical conductivity.

For the fabrication of a supercapacitor (SC) electrode, in general, the active material(s) is loaded on a suitable conductive substrate as a support. The challenge is selecting an ideal support for further deposition of the electroactive materials with large amount of loadings per unit area [6]. A substrate with the interconnected network and the hierarchical and porous structure enables enough electrolyte access to the active materials deposited on the substrate. In addition, the specific surface area with higher conductivity, higher mechanical stability and the flexibility of the substrate are key factors that offer higher power densities for the final device. So, the selected support plays a vital role in improving the efficiency in charge/discharge processes of SCs. In most of the researches in the field of batteries or supercapacitors, nickel foam or carbon cloth is used as substrate/support for loading the active materials. Nickel foam (NF) in supercapacitors acts as both good electrical conductive support and as the active capacitive material. The porous nature of NF backbone provides excellent mechanical strength and allows easy access of electrolyte for charge transportation.

Based on these issues, a large body of researches has been carried out to introduce a novel support or foam to increase the capacity as well as the power density of the fabricated SCs. Up to now, several foam electrodes including nickel foam [7,8], carbon nanotube (CNT) foam [9–11], hierarchically porous carbon foam [12,13], heteroatom engineered carbon foam [14], graphene (GR) foam [15,16] and GR/CNT hybrid foam [6] have been reported for their energy storage applications. These substrates/supports display their capacitive (in carbon-based) [17] and pseudo-capacitive (in Ni-based) behaviors. However, fabrication of the supports or foams based on metal oxides for their supercapacitive applications have rarely been reported yet. Recently, 3D porous metal oxide (V_2O_5, MoO_3, MnO_2) foams coated with nitrogen-doped carbon has been reported as suitable foams for their lithium storage applications [18]. Feng et al. have reported Fe—Mn oxide foams and studied their magnetic properties [19]. Very recently, Sesu et al. have fabricated a CoCuBi oxide foam structure as a significant electrocatalyst for methanol electrooxidation [20] and Han and Zhao have reported a novel iron oxide foam as acetone gas sensor [21].

For their supercapacitive applications, metal oxides provide higher specific capacitance because of their multiple oxidation states for the reversible Faradaic reactions and unique redox properties [22,23]. Compared to carbon materials, the advantage of metal oxide-based supercapacitor electrodes is their pseudo-capacitive behavior raising from their redox reactions. So, metal oxides with higher theoretical specific capacitance values such as RuO_2 [24,25], MnO_2 [26], NiO [27], and Co_3O_4 [28] have been widely investigated worldwide. However, among these metal oxides, the supercapacitive behavior of one-dimensional (1D) and two-dimensional (2D) ZnO nanostructures [29–31] have been investigated because of their high energy density, low cost, and eco-friendly nature. For example, carbon-ZnO nanocomposite has been reported recently as an appropriate supercapacitive material due to its high energy and power densities [32,33]. ZnO tetrapods have also been synthesized and proposed as a suitable supercapacitive electrode materials for its energy storage applications [34,35].

Although ZnO is one of the suitable material for its potential supercapacitor applications, it does suffer from a number of flaws including poor conductivity [36]. To address this limitation, several strategies were developed including the addition of conductive -material, the creation of porous structure and utilizing 3D structure [37–40]. Fabrication of 3D structure provides a large specific surface area with the increased capacity. In fact, it is expected that the interconnected network structure of 3D foam due to abundant porous at the surface, provides the improved electrode/electrolyte contact area, increases the ion contact sites, reduces the dead volume and shortens the ion diffusion processes [41,42].

In this work, regarding the above-mentioned issues on electron transfer rate, electrical conductivity, structure and the flexibility of the substrate in the supercapacitors, we have focused on the fabrication and introduction of a flexible 3D ZnO@C foam as a suitable substrate in energy storage devices. For this purpose, at first, the flower-like ZnO@C nanostructures were fabricated by using a simple hydrothermal method, and then, ZnO@C foam was fabricated by using a nickel foam as template. Significantly, the resulted foam does have high porosity to increase the ion contact sites and shorten the ion diffusion in the ionic transfer processes. Furthermore, the high conductivity of 3D ZnO@C foam leads to an improvement in the capacity and performance of the structure compared to a commercial nickel foam.

2. Experimental

2.1. Materials

All chemicals were of analytical grade. Deionized (DI) water was used throughout the work. Zinc nitrate hexahydrate, urea, *N*-methyl-2-pyrrolidone (NMP), polyvinylidene fluoride (PVDF), activated carbon (AC), isopropyl alcohol, tetraethyl orthosilicate (TEOS), ammonium hydroxide (NH_4OH), cetyltrimethylammonium bromide (CTAB), resorcinol, formaldehyde, hydrofluoric acid (HF), and hydrochloric acid (HCl) were purchased from Merck and used without purification.

2.2. Preparation of flower-like ZnO

The flower-like ZnO powder was synthesized by a simple hydrothermal method as reported elsewhere [43] with modification. Briefly, 0.30 g of $Zn(NO_3)_2 \cdot 6H_2O$ and 0.12 g of urea were dissolved in 70 mL deionized water and the resulted solution was gently mixed at room temperature for 30 min. Then, the mixture was transferred to a 50-mL Teflon-lined stainless steel autoclave and the autoclave was heated to 95 °C for 6 h. The resulted white precipitate was filtered and washed 3 times with ethanol and distilled water and dried overnight in an oven at 70 °C. Finally, ZnO powder was retrieved through a heat treatment at 300 °C in air for 2 h.

2.3. Preparation of ZnO@SiO_2@C

The core-shell structure of ZnO@SiO_2@C was synthesized via a sol-gel method. At first, the synthesized ZnO nanostructure was mixed in a solution containing 194 mL isopropyl alcohol, 18 mL DI water, 10 mL NH_4OH and 0.20 mL TEOS and stirred for 2 h at 40 °C. Then, 0.46 g of CTAB and 14.1 mL of deionized water were added to above-mentioned solution under the vigorous stirring condition. After 1 h stirring, 0.70 g of resorcinol, 56.4 mL of absolute ethanol, and 0.2 mL of NH_4OH were sequentially added to the solution. The resulting solution was then stirred for another 30 min at 35 °C and finally, 0.1 mL of formaldehyde was added. After the continual stirring and consequently polymerization via aging overnight, the obtained ZnO@SiO_2@RF nanospheres (RF: resorcinol-formaldehyde) were collected and washed several times with deionized water. The final product i.e. ZnO@SiO_2@C core-shell nanocomposite was prepared by the calcination of ZnO@SiO_2@RF powder at 600 °C for 3 h under the N_2 atmosphere (Scheme 1).

2.4. Fabrication of ZnO@C foam

For the fabrication of ZnO@C foam, a commercial nickel foam was used as a template for coating ZnO@SiO_2@C. Nickel foam (1×1 cm^2) was highly cleaned by consecutive sonication in DI water, ethanol, and acetone for 10 min and dried for 2 h at 60 °C. The paste for the fabrication of ZnO@C foam was prepared by mixing of synthesized ZnO@SiO_2@C powder as the backbone and PVDF as bonding agent with the mass ratios of 8:2 in NMP as solvent. The mixture was stirred for 12 h until a homogeneous slurry was obtained. Ni foam was gently coated by the

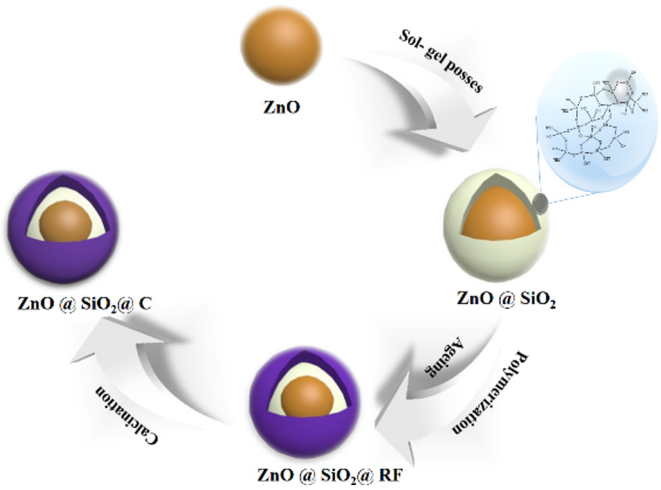

Scheme 1. Schematic representation of preparing ZnO@SiO_2@C composite.

resulted paste and dried at 60 °C for 12 h in an oven to obtain ZnO@SiO_2@C/Ni. Ni foam was chemically removed from ZnO@SiO_2@C/Ni by etching in 3 M HCl at 100 °C for 3 h. Then, the silica layer was etched by 1 M HF for 1 h [44–46]. Finally, the resulted 3D ZnO@C foam was dried at 60 °C for 12 h (Scheme 2).

2.5. Materials characterization

To identify the crystalline phase of the synthesized ZnO powder and the resulted ZnO@C foam, X-ray diffraction (XRD) spectrometer (Panalytical, X'Pert Pro system) with Cu K_α radiation (λ = 0.15418 nm) was used. The surface morphology of the flower-like ZnO and ZnO@C foam was characterized by field-emission scanning electron microscopy (FE-SEM, Tescan Mira3) equipped with energy-dispersive X-ray spectroscopy (EDX) analyzer.

2.6. Electrochemical measurements

The electrochemical characteristics of the samples were investigated by cyclic voltammetry (CV), galvanostatic charge-discharge, and electrochemical impedance spectroscopy (EIS) techniques by using a Galvanostat/Potentiostat Autolab PGSTATE 302 N (Metrohm Autolab, Switzerland) with a typical three-electrode electrochemical system including a Ni or ZnO@C foam as working electrode, an Ag/AgCl (KCl 3.0 M) as reference electrode and a Pt plate as counter electrode. Potassium hydroxide solution (KOH, 3.0 M) was used as an electrolyte in all of the electrochemical experiments. The asymmetrical supercapacitor was fabricated by assembling fabricated ZnO@C foam as the positive electrode and carbon clothes coated with 10 wt% activated carbon (AC) and 10 wt% PVDF binder (NMP as the solvent of material slurry) as the negative electrode. The polypropylene film was used as the separator which was soaked in 6 M KOH electrolyte.

3. Results and discussion

3.1. Characterization

The main challenge in the fabrication of ZnO@C foam by the proposed method is the possibility of ZnO corrosion in etching solution (HCl, 3 M) which is used for the removal of Ni foam. In fact, at the initial stages of this work, to fabricate ZnO@C foam, we synthesized ZnO@C powder. But, in the Ni foam chemical etching step, few amounts of ZnO from ZnO@C was dissolved in hot acidic solution. So, we designed to have a protective layer to prevent the dissolution of ZnO in the chemical etching step. The best choice was SiO_2-based protective layer. Therefore, ZnO@SiO_2@C core-shell nanocomposite was synthesized via the proposed three-step method. At first, ZnO nanostructure was synthesized by hydrothermal method. Then, a thin layer of SiO_2 was coated on ZnO via the conventional sol-gel method. The silica layer was coated on ZnO by the hydrolysis and condensation of TEOS in a mixture of water and ethanol in the presence of ammonia as a catalyst [47,48]. Finally, at the third step, ZnO@SiO_2 was coated with a polymeric layer of resorcinol-formaldehyde (RF) via a sol-gel process [49] and then, ZnO@SiO_2@RF was calcined under the inert atmosphere to obtain ZnO@SiO_2@C.

In the hydrothermal synthesis of flower-like ZnO, OH^- species through the coordination or electrostatic interactions can bind to Zn^{2+} to form $Zn(OH)_2$ and $Zn(OH)_4^{2-}$ (Eqs. (1) and (2)):

$$Zn^{2+} + 2OH^- \rightarrow Zn(OH)_2 \quad (1)$$

$$Zn(OH)_2 + 2OH^- \rightarrow Zn(OH)_4^{2-} \quad (2)$$

Then, ZnO is formed through the gradual dehydration of $Zn(OH)_4^{2-}$ (Eq. (3)) under the hydrothermal conditions:

$$Zn(OH)_4^{2-} \rightarrow ZnO + H_2O + 2OH^- \quad (3)$$

So, it seems that the gradual delivery of OH^- by urea (as an OH^- source precursor) in the process plays an important role in the formation of flower-like ZnO nanomaterials (Fig. 1a) [50], the fact that the FE-SEM images (Fig. 1b) and XRD pattern (Fig. 2) confirm the formation of high crystalline ZnO. The mechanism for the formation of flower-like ZnO nanomaterials is shown in Fig. 1. In the formation of flower-like ZnO, ZnO nanoneedles/nanosheets are connected together through the hydrothermal process to form ZnO spheres. Because of the large number of nanosheets/needles in this structure, it is expectd that the

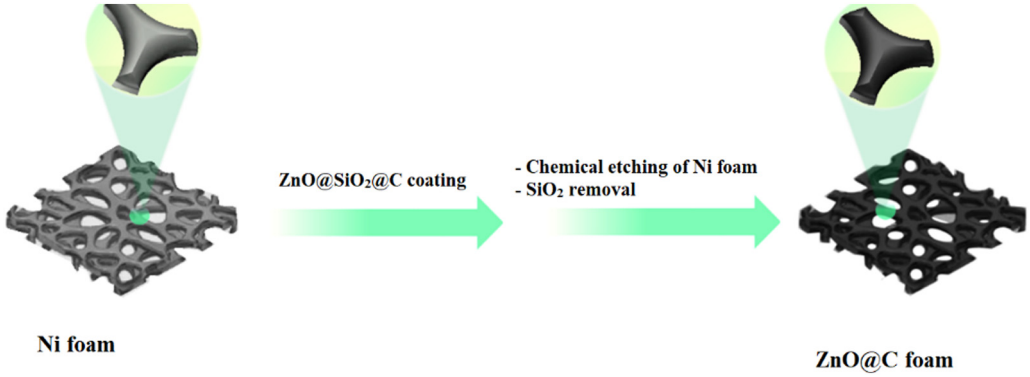

Scheme 2. Schematic representation of preparing ZnO@C foam.

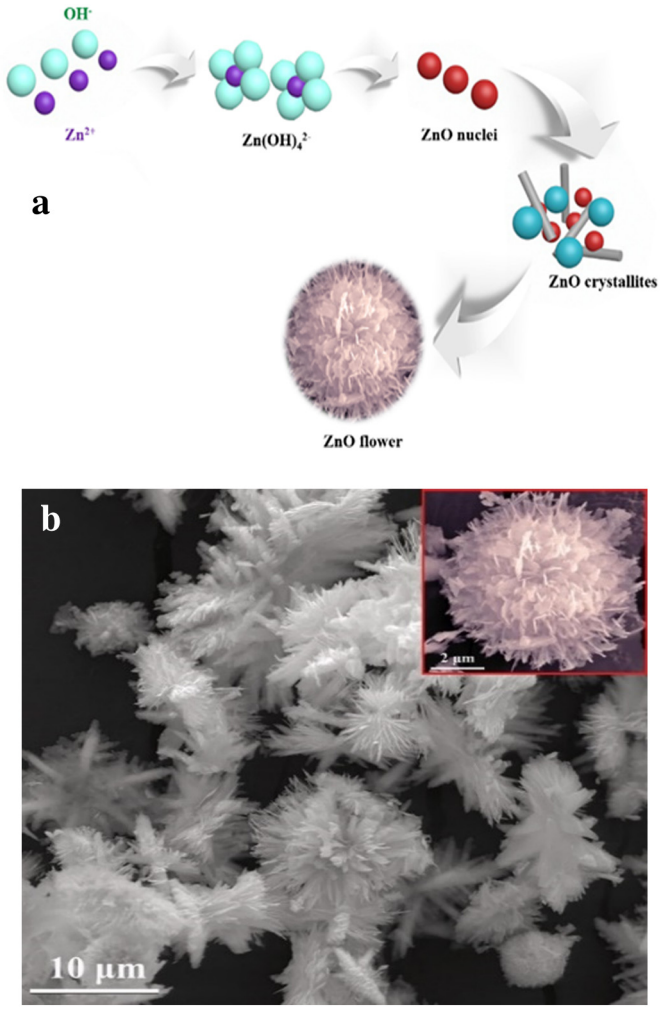

Fig. 1. (a) Schematic illustration of the formation process of flower-like ZnO, (b) FE-SEM images of synthesized ZnO.

electrochemical properties and the capacitive performance of the resulted electrode based on this material will be improved.

To investigate the thermal stability and the content of carbon in synthesized ZnO@SiO_2@C composite, thermal gravimetric analysis (TGA) was used in the temperature ranges from 25 °C to 700 °C under the ambient atmosphere at the ramp rate of 20 °C min^{-1} (Fig. 2a). The weight loss curve indicated that ZnO@SiO_2@C has suitable thermal stability, and carbon began to oxidize around 450 °C. The sharp decrease in the weight of composite after 450 °C confirms the presence of carbon in the structure.

Fig. 2b illustrates the XRD pattern of the flower-like ZnO@C. The characteristic diffraction peaks for ZnO is observed at 2θ values of 31.7°, 34.4°, 36.3°, 47.5°, 56.6°, 62.9°, 66.4°,67.9°, 69.1°, 72.6°, and 76.9°, attributed to (100), (002), (101), (102), (110), (103), (200), (112), (201), (004), and (202) planes, respectively. All diffraction peaks can be indexed to the hexagonal ZnO crystallites (JCPDS 36–1451) [51–53]. The sharp peaks for the sample confirm the high crystallinity of ZnO in the synthesized material.

After the chemical etching of SiO_2 layer by HF solution, ZnO@C foam was obtained. Fig. 3 shows the FE-SEM images of ZnO@ SiO_2@C and the fabricated ZnO@C foam. Fig. 3b shows that the ZnO@C foam has a 3D porous interconnected network structure and shows the original skeleton of the initial nickel foam template. The elemental mapping of the sample (Fig. 3c) indicates the uniform distribution of Zn and C elements in the fabricated foam. In addition, to have a quantitative analysis, the electron dispersive x-ray spectroscopy (EDX) of the foam was investigated (Fig. 3d) and the amount of Zn, O and C elements are obtained as 26.7, 23.1, and 50.2 wt%, respectively. The ratio of Zn and O is almost equal and the amount of C in the nanocomposite is higher than Zn and O. This indicates that flower-like ZnO particles are incorporated into carbon through resorcinol-formaldehyde reaction followed annealing. The flexibility of the fabricated ZnO foam was also examined 10 times without any destruction of the foam skeleton (Fig. 3e) indicating its potential applications in the flexible supercapacitors.

The thickness of the fabricated foam was 1.32 mm. By using the four-point probe measurement, the results (Table 1) indicate that the electrical conductivity of the fabricated ZnO@C foam is high (3.26×10^{-2} S cm^{-1}) with low resistivity of about 31 Ω cm. The electrical conductivity of fabricated ZnO@C foam is lower than that of graphene foam (for example, 1 S cm^{-1}) [54] and CNT/graphene foam (for example, 1.9 S cm^{-1}) [6]. The lower electrical conductivity of ZnO@C foam is due to the lower conductivity of ZnO as semiconducting material compared to graphene or carbon nanotube (CNT). As will be discussed in folowing sections, the lower electrical conductivity of the fabricated foam is compensated with fast electron transfer rate, pseudocapacitance behavior and higher capacitance of foam without any modification with other catalytic or capacitive compounds.

3.2. Electrochemical analysis

For the investigation of the electrochemical characteristics of ZnO@C foam, it was firstly carried out with a standard three-electrode system in 3.0 M KOH aqueous electrolyte at room temperature. Cyclic voltammogram (CV) of the ZnO@C foam at the scan rate of 20 mV s^{-1} in the potential window from 0 to 0.6 V is shown in Fig. 4a. CV of a commercial Ni foam was also involved in Fig. 4a. A pair of Faradaic redox peaks occurred around 0.35 V and 0.15 V vs. Ag/AgCl (as a reference electrode) corresponding to the oxidation and reduction processes, respectively. These redox peaks stem from the intercalation and de-intercalation of cationic alkali metal K^+ from the electrolyte into ZnO@C structure. The reaction at the electrode surface can be represented as follows (Eq. (4)) [55–57]:

$$ZnO + K^+ + e^- \leftrightarrow ZnOK \tag{4}$$

The difference between the oxidation (E_{pa}) and reduction (E_{pc}) peak potentials (ΔE_p) is about 0.2 V, indicating the quasi-reversible behaviour of the electrochemical reaction at the electrode surface (Eq. (4)) with the accelerated charge transfer rates, the fact that will be discussed in the following section based on the electrochemical impedance spectroscopic (EIS) data.

The oxidation and reduction peak currents are high enough to confirm its higher surface area, easier intercalation/de-intercalation of K^+ into ZnO@C nanostructure, as well as its higher conductivity. CV of Ni foam is also included in Fig. 4a. The oxidation and reduction peak currents of proposed ZnO@C foam are higher than that of Ni foam. Cyclic voltammograms of ZnO@C foam were also investigated at different scan rates (Fig. 4b). With the increase in the scan rate (ν), the currents are increased and the oxidation and reduction peak potentials shift to more and less positive potential values, respectively, indicating the quasi-reversible behavior of the electrode [58].

The specific capacitance values of the ZnO@C foam derived from the voltammograms at different scan rates were calculated as follows (Eq. (5)) [37]:

$$C = \frac{1}{v\,(V_c - V_a)} \int_{V_a}^{V_c} J\,(V)\,dV \tag{5}$$

where C, ν, V_c, V_a and J are the specific capacitance (F cm^{-2}), scan rate (V s^{-1}), high and low potential limit (V), and instant current density (A cm^{-2}), respectively. Fig. 4c illustrates the plot of specific capacitance

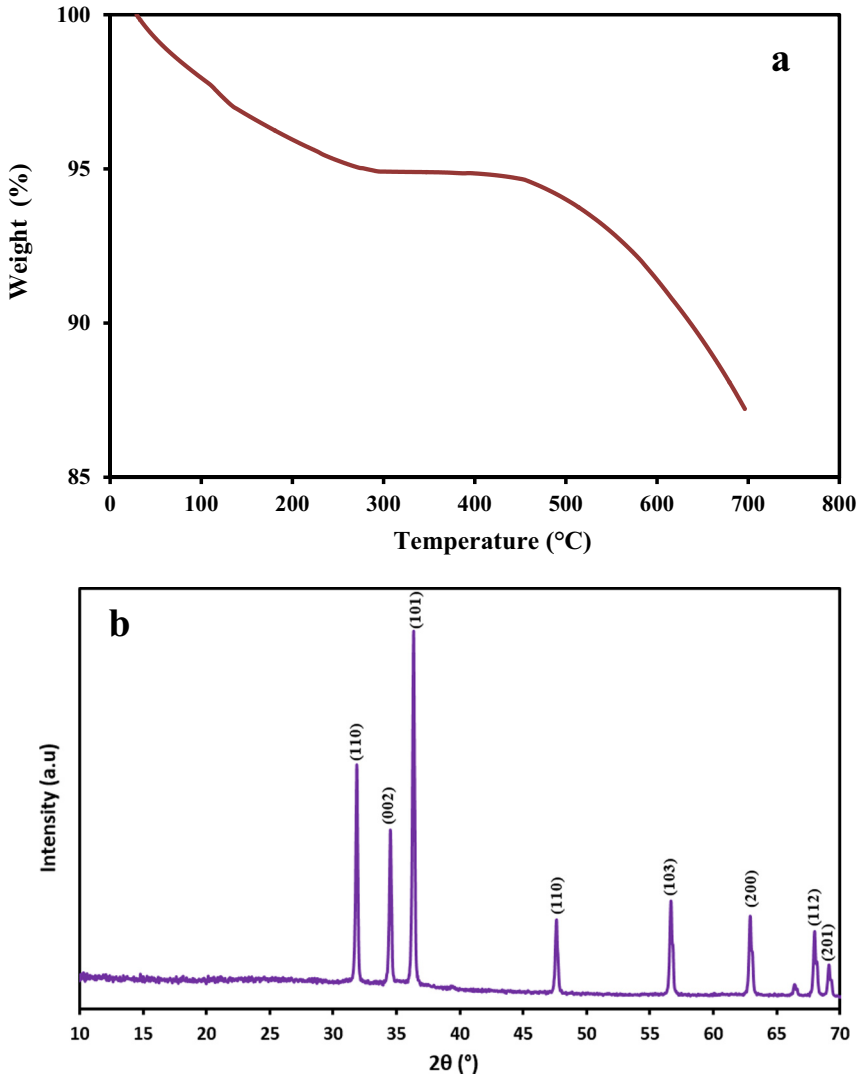

Fig. 2. (a) TGA curve of ZnO@SiO_2@C nanocomposite, (b) XRD pattern of ZnO@C powder.

of ZnO@C foam as a function of scan rate. The graph shows a gradual decrease in the specific capacitance with the increase of scan rate. It means that at the lower scan rates, the electrolyte ions easily penetrate into almost all of the active cites of ZnO@C foam, while at higher scan rates, the ion diffusion is limited to the accessible active cites for charge storage [1,37].

To examine the practical applications of ZnO@C foam in supercapacitors, the galvanostatic charge-discharge (GCD) curves in the potential range of 0 to 0.45 V was investigated at the current density of 4 mA cm^{-2} (Fig. 4d). The GCD curve of Ni foam was also included in the plot, which was obtained under the same conditions. The charge and discharge parts of GCD curve for ZnO@C foam keep the symmetric relation, indicating the excellent reversibility of the redox reaction as well as good electrochemical behavior, which confirms the CV results (Fig. 4a). Low IR drop in GCD curve of ZnO@C foam offers the lower electrode-electrolyte interfacial resistance which is an important factor in the improvement of a supercapacitor performance. Generally, the foam acts as hybrid capacitor and the mechanism of charge and discharge contains two different parts. In the potential range of 0.4 V to 0.2 V, the decay in discharge part indicates the occurrence of electrochemical process (pseudocapacitance), while in the potential range of 0.2 V to 0 V, the decay is from the discharge of double layer (EDL capacitance). The specific capacitance of an electrode is calculated by using the following equation (Eq. (6)) [38]:

$$C_{sc} = \frac{Jt}{\Delta V} \tag{6}$$

where C_{sc}, J, t and ΔV are the specific capacitance (mF cm^{-2}), discharge current density (mA cm^{-2}), discharge time (s), and the potential range of charge-discharge (V), respectively. The specific capacitances (C_{sc}) of both ZnO@C and Ni foams at 4 mA cm^{-2} are reported in Table 2. The energy density (E, Wh m^{-2}) and power density (P, Wm^{-2}) of both electrodes have also been depicted in Table 2. A suitable electrochemical supercapacitor is expected to provide a high specific capacitance as well as the high energy density. The equations that describe E and P are as follows (Eqs. (7) and (8)): [38,59].

$$E = \frac{1}{2} C_{cs} \Delta V^2 \tag{7}$$

$$P = \frac{E}{\Delta t} \tag{8}$$

where E, P, C_{cs}, ΔV, and Δt are the energy density (Wh m^{-2}), power density (Wm^{-2}), specific capacitance (F cm^{-2}), potential window (ΔV), and discharge time (s), respectively. Based on the results obtained

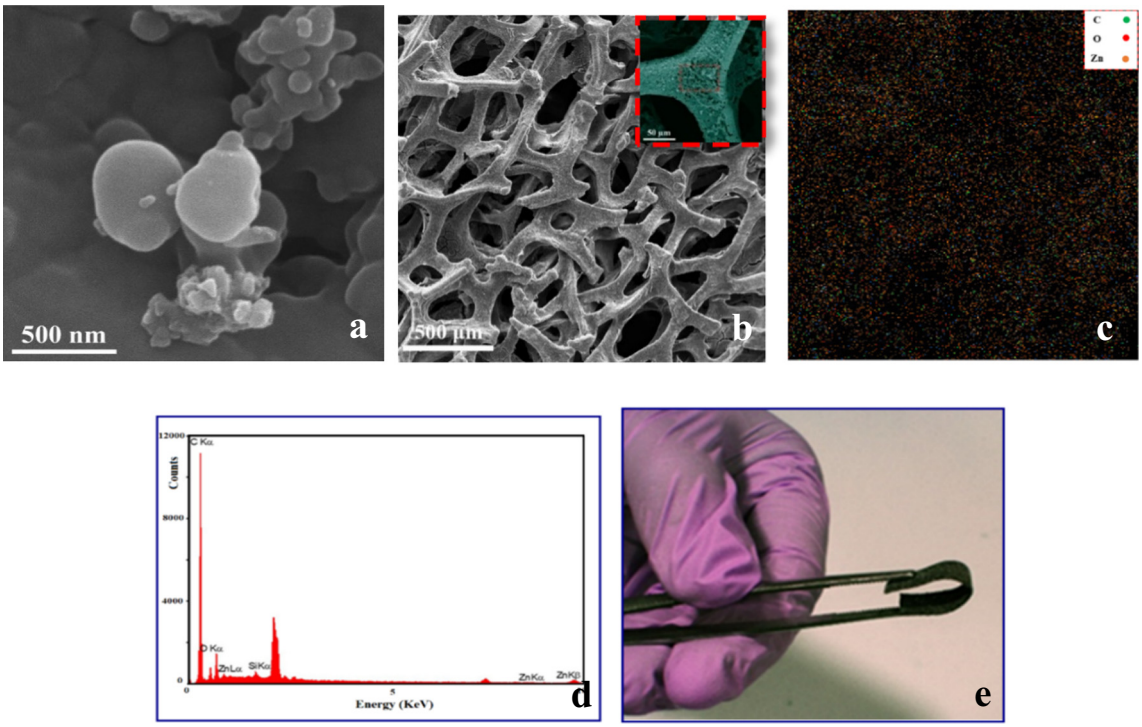

Fig. 3. (a) FE-SEM image of ZnO@SiO_2@C; (b) FE-SEM image, (c) elemental mapping, (d) EDX spectrum, and (e) photograph of the fabricated flexible ZnO@C foam.

by a three-electrode electrochemical system (Table 2), the specific capacitance of ZnO@C foam is higher than that of Ni foam. This discrepancy is mainly due to the high conductivity, large surface area and the higher pore volume in ZnO@C foam compared to Ni foam. Any improvement in these physical properties would increase the interaction between the electrode and electrolyte through the pores and decrease the ion transport pathway [37]. Also, the specific energy density and the power density of ZnO@C foam is higher than that of Ni foam. So, it can be concluded that ZnO@C foam due to its high specific capacitance, high energy and power densities (Table 2) with high conductivity and lower resistivity (Table 1) can be used as an alternative substrate for the fabrication of supercapacitor electrodes.

The GCD curves of ZnO@C foam at various current densities are shown in Fig. 5a. The GCD curves of ZnO@C foam exhibited a triangular shape. The quasi-symmetric GCD curves indicate that the ZnO@C foam has highly reversible faradaic reactions. The specific capacitances of 1298, 1120, 1005, and 906 mF cm^{-2} were obtained at the discharge current densities of 2, 4, 6, and 8 mA cm^{-2}, respectively. The specific capacitances of ZnO@C foam can be calculated from GCD curves according to Eq. (6). As shown in Fig. 6b, the specific capacitance of ZnO@C foam is gradually decreased with the increase of current density.

In Table 3, the specific capacitances of the fabricated ZnO@C foam and carbon-ZnO electrodes have been compared and it can be concluded that the proposed foam show superior supercapacitive performance among the summarised reported values.

3.3. Electrochemical impedance spectroscopy

In order to get more insight into charge transfer resistance, the electrochemical impedance spectroscopy (EIS) of ZnO@C foam was studied. EIS is a powerful electrochemical technique for studying the charge transfer rate in supercapacitor electrodes. Fig. 6a shows the Nyquist plots for ZnO@C and Ni foams obtained in open circuit voltage in the frequency range of 0.1 Hz to 100 kHz. Also, Fig. 6b shows the Bode plot of the foam. In terms of the frequency region, the impedance spectra may be classified into high-frequency redox reaction, mid-frequency diffusion process and low-frequency capacitive phenomena. The mid-frequency region in Nyquist plot of ZnO@C foam indicates the appropriate diffusion rate of electrolyte ions from the electrolyte to the electrode, which depends on the various physical factors including the porosity of the active material, morphology and the thickness of deposited active material at the electrode surface. Further, in this region, compared to Ni foam, the Nyquist plot of ZnO@C foam displays a sharp rise of impedance, indicating a good capacitive behaviour of the fabricated foam. In low-frequency region, ZnO@C foam shows the capacitive behaviour, and at the high-frequency region, shows the appropriate electrical conductivity at the electrode-electrolyte interface. By fitting the data of the Nyquist plot, the charge transfer resistance (R_{ct}) of ZnO@C and Ni foams were obtained to be 7.1 Ω and 10.3 Ω, respectively.

The Bode plots of the foam were also investigated (Fig. 6b).

In general, the impedance characteristics of a supercapacitor oscillate between a phase angle of 0° (pure resistor) to 90° (pure capacitor). So, the phase angle for the ideal capacitor is 90° and when the phase angle of the electrode approaches 90°, the device is an ideal capacitor. The Bode plots of both foams show that the phase angle of the fabricated ZnO@C foam reaches 77°, which is greater than that of Ni foam (bout 73°).

From the scrutiny of the frequency response of the foams, the response time (τ_{rs}) of both foams can be calculated from the frequency values (f) at the phase angle of 45° by using the following equation (Eq. (9)):

$$\tau_{rs} = \frac{1}{2\pi f} \tag{9}$$

τ_{rs} for Ni and ZnO@C foams were obtained as 20 ms and 7 ms, respectively. The lower τ_{rs} value for latter indicates the fast electron transfer and more conductivity for ZnO@C foam [64,65].

Table 1
Four-point probe measurement of the conductivity of ZnO@C foam.

Sample	Resistance (Ω)	Resistivity (Ω cm)	Conductivity (S cm^{-1})
ZnO@C foam	2.71	31	3.26×10^{-2}

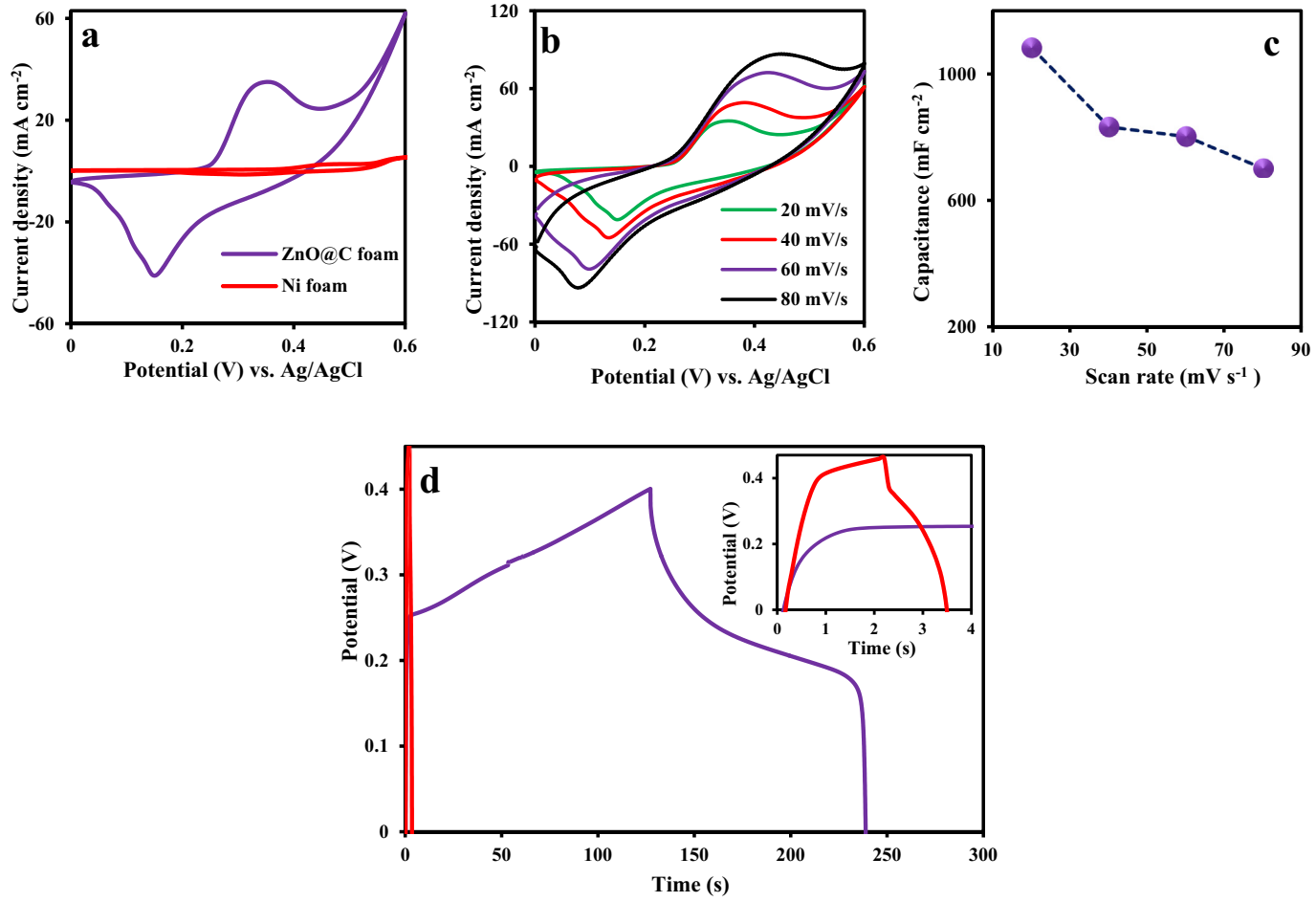

Fig. 4. (a) Cyclic voltammograms of ZnO@C foam and Ni foam in 3.0 M KOH at the scan rate of 20 mV s^{-1}, (b) cyclic voltammograms of ZnO@C foam at different scan rates of 20, 40, 60 and 80 mV s^{-1}, c) plot of the specific capacity of ZnO@C foam versus scan rate, and d) charge-discharge curves of ZnO@C foam (Blue line) and Ni foam (Redline) at the current density of 4 mA cm^{-2} in 3.0 M KOH. (For interpretation of the references to colour in this figure legend, the reader is referred to the web version of this article.)

The complex capacitance calculations for foam were also performed. The frequency dependent complex capacitance (C_{SC}) can be defined as a combination of real and imaginary parts of the capacitance, C′ and C″, and is calculated by Eqs. (10)–(12) [64]:

$$C_{SC} = C\prime + C'' \tag{10}$$

where:

$$C\prime = \frac{(-Z'')}{\omega\,|Z|^2} \tag{11}$$

$$C'' = \frac{(-Z')}{\omega\,|Z|^2} \tag{12}$$

where, Z′, Z″ and |Z| are the real, imaginary and modulus of total impedance of the capacitance, respectively.

Fig. 6c illustrates the frequency response for the real part of ZnO@C and Ni foams. Actually, the real part of the capacitance indicates the variation of capacitance created via electrolyte ion penetration inside the pores of foam at a particular frequency. At low frequencies, due to the ion penetration into deep pores, the real part of the capacitance of ZnO@C foam, C′, is increased. However, at high frequencies, C′ decreased because of the limited ion access the surface of the pores. In these high frequencies, the real capacitance, due to the resistor behaviour of the foam, is very low and is independent of frequency. Therefore, the amount of capacitance stored in the foam should be measured at low frequency values. As Fig. 6c shows, in all low-frequency ranges, ZnO@C foam has significantly higher capacitances compared to Ni foam, mainly due to the higher conductivity of the former. As a result, ZnO@C foam has a suitable superconducting performance than Ni foam.

The changes in the imaginary capacitance, C″, with change in frequency for ZnO@C and Ni foams are also shown in Fig. 6d. The dielectric relaxation time (τ_o) can be calculated from $\tau_o = \frac{1}{f}$, where f is the frequency at which C″ is in its maximum values. So, τ_o represents the minimum time required for the discharge of all stored energy in the foam. The results show that ZnO@C foam reaches to τ_o faster than Ni foam, indicating the excellent capacitive behavior of ZnO@C foam.

Finally, to evaluate the practical advantage of the fabricated ZnO@C foam for supercapacitor purposes, the asymmetric supercapacitor (ASC) was fabricated by using ZnO@C foam and active carbon as the positive and negative electrodes, respectively. At first, cyclic voltammetry was performed in a three electrode system to find the electrochemical potential windows of the positive and negative electrodes (Fig. 7a). As the results show, the potential windows are in the ranges of −1.0 V

Table 2
Specific capacitance, energy density and power density of Ni and ZnO@C foams.

Foam	Current density (mA cm^{-2})	Specific capacitance (mF cm^{-2})	Energy density (Wh m^{-2})	Power density (W m^{-2})
Ni	4	13.6	1.5	0.93
ZnO@C	4	1120	224	2.17

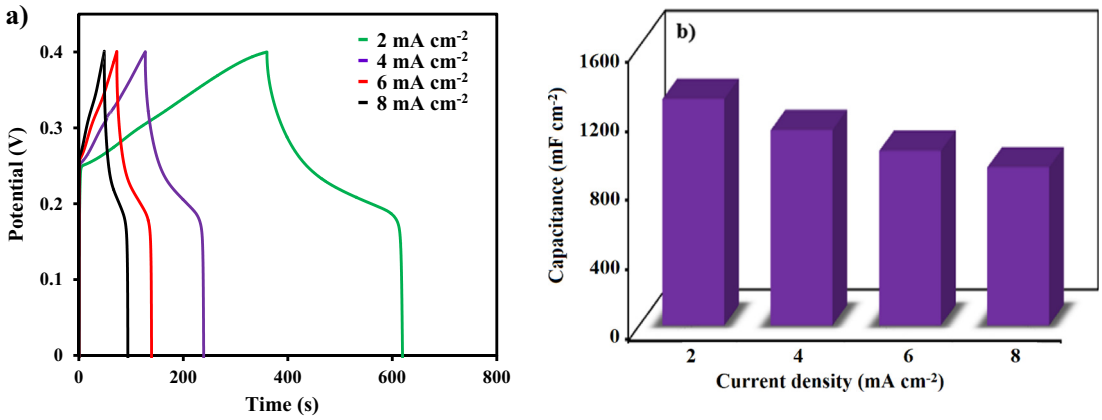

Fig. 5. (a) GCD curves and (b) the specific capacitances of ZnO@C foam at various current densities of 2, 4, 6 and 8 mA cm^{-2}.

to 0.0 V for negative electrode and 0.0 V to +0.6 V for positive electrode and the capacitances of two electrodes are almost equal. The working potential window of 0 to 1.2 V was selected, where the oxidation/reduction of water at the end of potential window was not occurred and the transport of charge density was higher. The voltammetric responses of ASC were also investigated at different scan rates in the capacitive potential range of 0.0 to 1.2 V (Fig. 7b). By the increase in the scan rate, ZnO@C foam//AC shows an excellent areal capacitance with increased current density and without considerable changes in the shape of the curves.

Fig. 7c illustrates GCD profiles of the ZnO@C foam//AC device at the various current densities from 4 to 10 mA cm^{-2}. The low Ohmic drops of ZnO@C foam//AC demonstrate the excellent rate capability and low internal resistance. In addition, ZnO@C foam//AC illustrates a specific capacitance of 189.34 F cm^{-2} at a current density of 4 mA cm^{-1}, which shows suitable supercapacitor behavior. The Nyquist plot of the ZnO@C foam//AC device is shown in Fig. 7d. In low-frequency region, a sharp rise of impedance is observed, indicating the excellent performance of ZnO@C foam//AC asymmetric supercapacitor. A slight change in the Nyquist plot of the ZnO@C foam//AC after 1000 cycles indicates

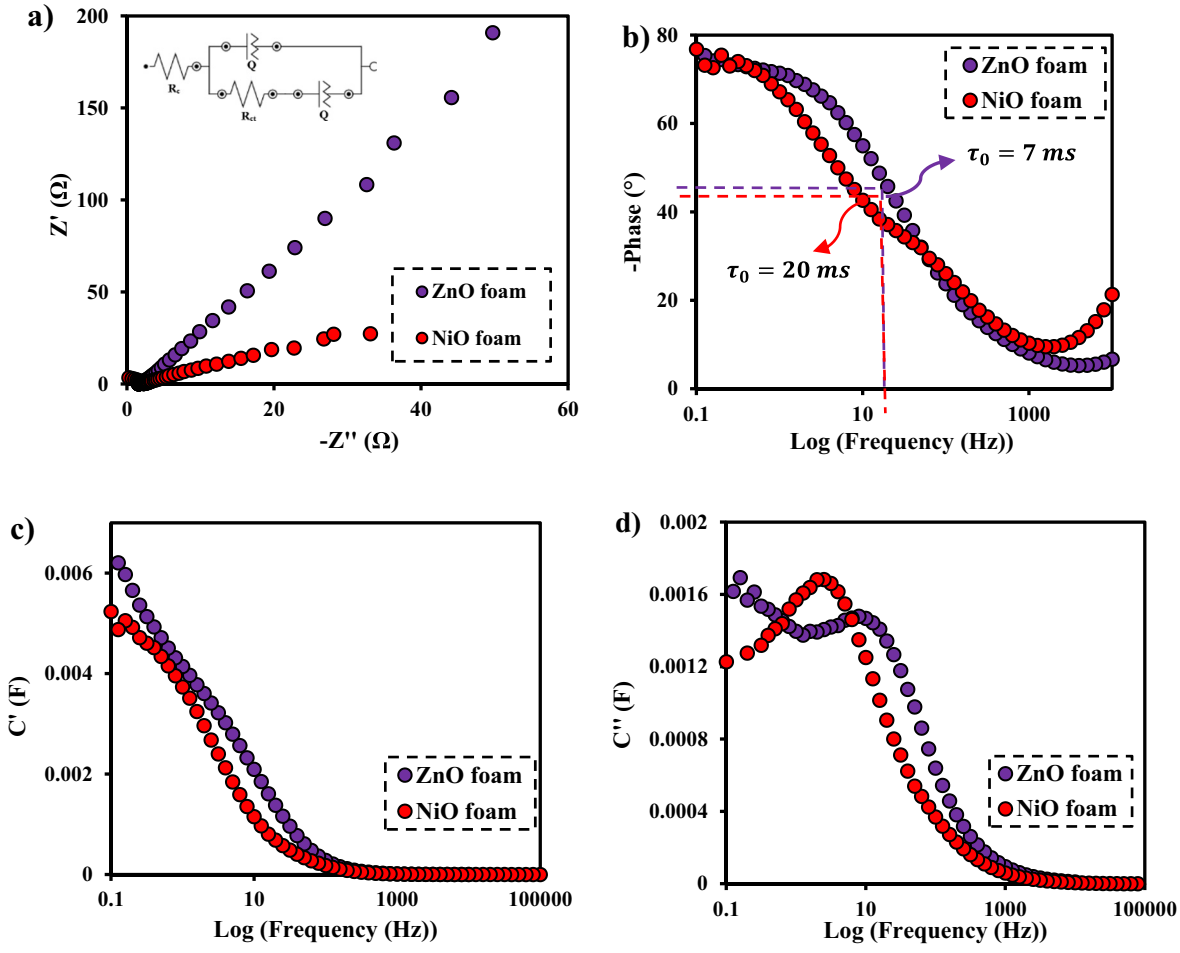

Fig. 6. (a) Nyquist plots, equivalent circuit diagram and (b) Bode plots of ZnO@C and Ni foams. (c) Real capacitance, and (d) imaginary capacitance as a function of frequency for ZnO@C and Ni foams.

Table 3
Comparison of the electrochemical performance of ZnO@C foam with previous reports.

Electrode/foam	Scan rate or current density	Specific capacaince	Electrolyte	Ref.
Carbon sphere@ZnO	2 A g^{-1}	630 F g^{-1}	6 M KOH	[60]
ZnO/RGO/ZnO	5 mV s^{-1}	275 F g^{-1}	1 M Na_2SO_4	[61]
RGO/ZnO	5 mV s^{-1}	312 F g^{-1}	1 M Na_2SO_4	[62]
GR/ZnO	5 mV s^{-1}	109 F g^{-1}	1 M KCl	[63]
ZnO@C foam	4 mA cm^{-2}	1120 mF cm^{-2}	3 M KOH	**This work**

the excellent cycle stability and suitable performance of the ZnO@C foam//AC.

Fig. 7e illustrates the cycling stability of the ZnO@C foam//AC supercapacitor device for 3000 cycles at 20 mA cm^{-2}. The obtained results show that the fabricated device exhibits high stable cycling performance and reversible capacity. After 3000 cycles, the assembled device has retained 95.8% of its initial capacitance. The excellent cycle stability is attributed to the excellent ion conduction due to the high surface area and a large number of porous on the ZnO@C foam surface.

4. Conclusions

The excellent electrochemical performance of the proposed flexible ZnO@C foam promises its potential applications in energy production and storage devices. In comparison with commercially available Ni foam and synthesized metal oxide electrodes, the fabricated ZnO@C foam provides a high areal specific capacitance of 1120 mF cm^{-2} at a current density of 4 mA cm^{-2}. Due to the high conductivity of the fabricated ZnO@C foam, the efficiency of the charge/discharge processes was improved. In addition, the porous structure of ZnO@C foam leads to the creation of a convenient path for ion transportation which accelerates the reversible faradaic reaction. The 3D structure of ZnO@C foam leads to the creation of a large surface area which increases the contacts between the electrolyte and active materials and supplies more accessible active sites for the electrochemical reactions. Finally, due to the remarkable electrochemical properties including improved capacitance, high electron transfer rate and conductivity as well as the flexibility of ZnO@C foam, it is expected that the proposed foam benefits high potential applicability in energy storage and production devices.

CRediT authorship contribution statement

Zohre Fahimi: Conceptualization, Data curation, Formal analysis, Investigation, Methodology, Writing - original draft. **Omran Moradlou:** Project administration, Supervision, Validation, Writing-review & editing.

Declaration of competing interest

The authors declare that they have no known competing financial interests or personal relationships that could have appeared to influence the work reported in this paper.

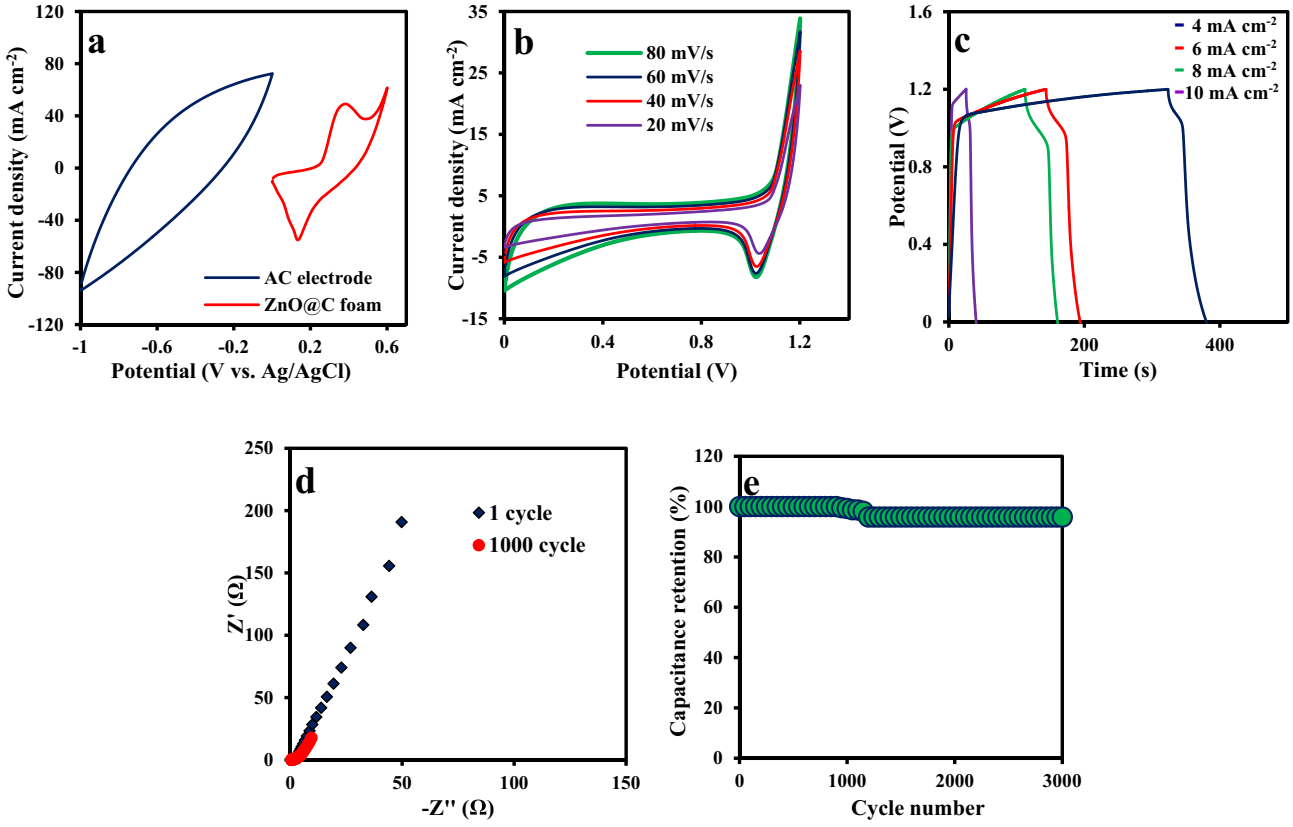

Fig. 7. Electrochemical characteristics of the fabricated asymmetric supercapacitor ZnO@C foam//AC: (a) CVs of ZnO@C foam (positive) and AC (negative) electrodes in a three-electrode cell in 6.0 M KOH at a scan rate of 20 mV s^{-1}, (b) CVs of ZnO@C foam//AC at the scan rates of 20, 40, 60 and 80 mV s^{-1}, (c) GCD curves of a ZnO@C foam//AC at different current densities of 4, 6, 8 and 10 mA cm^{-2}, d) Nyquist plot of ZnO@C foam//AC at the 1st and 1000th cycles, and e) the cycling profile of ZnO@C foam//AC at the current density of 20 mA cm^{-2}.

Acknowledgements

The authors would like to thank Research Council of Alzahra University for financial support.

References

[1] J. Jayachandiran, J. Yesuraj, M. Arivanandhan, A. Raja, S.A. Suthanthiraraj, R. Jayavel, D. Nedumaran, Synthesis and electrochemical studies of rGO/ZnO nanocomposite for supercapacitor application, J. Inorg. Organomet. Polym. Mater. (2018) 1–10.
[2] B. Pant, M. Park, G.P. Ojha, J. Park, Y.-S. Kuk, E.-J. Lee, H.-Y. Kim, S.-J. Park, Carbon nanofibers wrapped with zinc oxide nano-flakes as promising electrode material for supercapacitors, J. Colloid Interface Sci. 522 (2018) 40–47.
[3] D. Song, J. Zhu, J. Li, T. Pu, B. Huang, C. Zhao, L. Xie, L. Chen, Free-standing two-dimensional mesoporous ZnCo2O4 thin sheets consisting of 3D ultrathin nanoflake array frameworks for high performance asymmetric supercapacitor, Electrochim. Acta 257 (2017) 455–464.
[4] S.R. Kwon, J. Harris, T. Zhou, D. Loufakis, J.G. Boyd, J.L. Lutkenhaus, Mechanically strong graphene/aramid nanofiber composite electrodes for structural energy and power, ACS Nano 11 (7) (2017) 6682–6690.
[5] G. Yu, X. Xie, L. Pan, Z. Bao, Y. Cui, Hybrid nanostructured materials for high-performance electrochemical capacitors, Nano Energy 2 (2) (2013) 213–234.
[6] J. Liu, L. Zhang, H.B. Wu, J. Lin, Z. Shen, X.W.D. Lou, High-performance flexible asymmetric supercapacitors based on a new graphene foam/carbon nanotube hybrid film, Energy Environ. Sci. 7 (11) (2014) 3709–3719.
[7] G. Zhu, H. Wen, M. Ma, W. Wang, L. Yang, L. Wang, X. Shi, X. Cheng, X. Sun, Y. Yao, A self-supported hierarchical Co-MOF as a supercapacitor electrode with ultrahigh areal capacitance and excellent rate performance, Chem. Commun. 54 (74) (2018) 10499–10502.
[8] H. Chen, S. Zhou, L. Wu, Porous nickel hydroxide–manganese dioxide-reduced graphene oxide ternary hybrid spheres as excellent supercapacitor electrode materials, ACS Appl. Mater. Interfaces 6 (11) (2014) 8621–8630.
[9] R. Paul, V. Etacheri, V.G. Pol, J. Hu, T.S. Fisher, Highly porous three-dimensional carbon nanotube foam as a freestanding anode for a lithium-ion battery, RSC Adv. 6 (83) (2016) 79734–79744.
[10] Y. Cui, M. Zhang, Fabrication of cross-linked carbon nanotube foam using polymethylmethacrylate microspheres as templates, J. Mater. Chem. A 1 (44) (2013) 13984–13988.
[11] L. Ma, R. Liu, H. Niu, L. Xing, L. Liu, Y. Huang, Flexible and freestanding supercapacitor electrodes based on nitrogen-doped carbon networks/graphene/bacterial cellulose with ultrahigh areal capacitance, ACS Appl. Mater. Interfaces 8 (49) (2016) 33608–33618.
[12] Y. Wang, D. Kong, S. Huang, Y. Shi, M. Ding, Y. Von Lim, T. Xu, F. Chen, X. Li, H.Y. Yang, 3D carbon foam-supported WS 2 nanosheets for cable-shaped flexible sodium ion batteries, J. Mater. Chem. A 6 (23) (2018) 10813–10824.
[13] Z. Cao, J. Zhang, Y. Ding, Y. Li, M. Shi, H. Yue, Y. Qiao, Y. Yin, S. Yang, In situ synthesis of flexible elastic N-doped carbon foam as a carbon current collector and interlayer for high-performance lithium sulfur batteries, J. Mater. Chem. A 4 (22) (2016) 8636–8644.
[14] H. Peng, B. Yao, X. Wei, T. Liu, T. Kou, P. Xiao, Y. Zhang, Y. Li, Pore and heteroatom engineered carbon foams for supercapacitors, Adv. Energy Mater. 9 (19) (2019), 1803665.
[15] L. Zhang, D. DeArmond, N.T. Alvarez, D. Zhao, T. Wang, G. Hou, R. Malik, W.R. Heineman, V. Shanov, Beyond graphene foam, a new form of three-dimensional graphene for supercapacitor electrodes, J. Mater. Chem. A 4 (5) (2016) 1876–1886.
[16] X. Xia, D. Chao, C.F. Ng, J. Lin, Z. Fan, H. Zhang, Z.X. Shen, H.J. Fan, VO 2 nanoflake arrays for supercapacitor and Li-ion battery electrodes: performance enhancement by hydrogen molybdenum bronze as an efficient shell material, Mater. Horiz. 2 (2) (2015) 237–244.
[17] Z. Tang, G. Zhang, H. Zhang, L. Wang, H. Shi, D. Wei, H. Duan, MOF-derived N-doped carbon bubbles on carbon tube arrays for flexible high-rate supercapacitors, Energy Storage Materials 10 (2018) 75–84.
[18] K. Lu, J. Xu, J. Zhang, B. Song, H. Ma, General preparation of three-dimensional porous metal oxide foams coated with nitrogen-doped carbon for enhanced lithium storage, ACS Appl. Mater. Interfaces 8 (27) (2016) 17402–17408.
[19] Y. Feng, J. Fornell, H. Zhang, P. Solsona, M. Baró, S. Suriñach, E. Pellicer, J. Sort, Synthesis of α-Fe2O3 and Fe-Mn oxide foams with highly tunable magnetic properties by the replication method from polyurethane templates, Materials 11 (2) (2018) 280.
[20] D.C. Sesu, P. Marbaniang, S. Ingavale, A.C. Manohar, B. Kakade, Bi-Co-Cu metal oxide foam as significant electrocatalyst for methanol electrooxidation, ChemistrySelect 5 (1) (2020) 306–311.
[21] D. Han, M. Zhao, Facile and simple synthesis of novel iron oxide foam and used as acetone gas sensor with sub-ppm level, J. Alloys Compd. 815 (2020), 152406.
[22] R.B. Rakhi, W. Chen, D. Cha, H.N. Alshareef, High performance supercapacitors using metal oxide anchored graphene nanosheet electrodes, J. Mater. Chem. 21 (40) (2011) 16197–16204.
[23] J.H. Kim, S. Lee, J. Choi, T. Song, U. Paik, Stackable, three dimensional carbon–metal oxide composite for high performance supercapacitors, J. Mater. Chem. A 3 (41) (2015) 20459–20464.
[24] Q. Wang, X. Liang, Y. Ma, D. Zhang, Fabrication of hollow nanorod electrodes based on RuO 2//Fe 2 O 3 for an asymmetric supercapacitor, Dalton Trans. 47 (23) (2018) 7747–7753.
[25] Y. Yang, Y. Liang, Y. Zhang, Z. Zhang, Z. Li, Z. Hu, Three-dimensional graphene hydrogel supported ultrafine RuO 2 nanoparticles for supercapacitor electrodes, New J. Chem. 39 (5) (2015) 4035–4040.
[26] S. Mardi, O. Moradlou, A.Z. Moshfegh, Fabrication and the electrochemical activation of network-like MnO 2 nanoflakes as a flexible and large-area supercapacitor electrode, J. Solid State Electrochem. 22 (11) (2018) 3507–3514.
[27] Y. Liu, Y. Wang, H. Wang, P. Zhao, H. Hou, L. Guo, Acetylene black enhancing the electrochemical performance of NiCo-MOF nanosheets for supercapacitor electrodes, Appl. Surf. Sci. 492 (2019) 455–463.
[28] O. Moradlou, H. Ansarinejad, M. Hosseinzadeh, H. Kazemi, High-performance solid state asymmetric supercapacitor based on electrochemically decorated 3D network-like Co3O4 architecture on NiO nanoworms, J. Alloys Compd. 755 (2018) 231–241.
[29] D. Mohapatra, S. Parida, S. Badrayyana, B.K. Singh, High performance flexible asymmetric CNO-ZnO//ZnO supercapacitor with an operating voltage of 1.8 V in aqueous medium, Appl. Mater. Today 7 (2017) 212–221.
[30] S.K. Singh, V.M. Dhavale, R. Boukherroub, S. Kurungot, S. Szunerits, N-doped porous reduced graphene oxide as an efficient electrode material for high performance flexible solid-state supercapacitor, Appl. Mater. Today 8 (2017) 141–149.
[31] G. Zhang, Y. Song, H. Zhang, J. Xu, H. Duan, J. Liu, Radially aligned porous carbon nanotube arrays on carbon fibers: a hierarchical 3D carbon nanostructure for high-performance capacitive energy storage, Adv. Funct. Mater. 26 (18) (2016) 3012–3020.
[32] M. Sun, J. Wang, M. Xu, Z. Fang, L. Jiang, Q. Han, J. Liu, M. Yan, Q. Wang, H. Bi, Hybrid supercapacitors based on interwoven CoO-NiO-ZnO nanowires and porous graphene hydrogel electrodes with safe aqueous electrolyte for high supercapacitance, Advanced Electronic Materials 5 (12) (2019), 1900397.
[33] S. Chaudhary, L.S. James, A.K. Kumar, C.V. Ramana, D. Mishra, S. Thomas, D. Kim, Reduced graphene oxide/ZnO nanorods nanocomposite: structural, electrical and electrochemical properties, J. Inorg. Organomet. Polym. Mater. (2019) 1–9.
[34] Q. Luo, P. Xu, Y. Qiu, Z. Cheng, X. Chang, H. Fan, Synthesis of ZnO tetrapods for high-performance supercapacitor applications, Mater. Lett. 198 (2017) 192–195.
[35] G. Wu, Y. Song, J. Wan, C. Zhang, F. Yin, Synthesis of ultrafine ZnO nanoparticles supported on nitrogen-doped ordered hierarchically porous carbon for supercapacitor, J. Alloys Compd. 806 (2019) 464–470.
[36] N. Sinan, E. Unur, Fe3O4/carbon nanocomposite: investigation of capacitive & magnetic properties for supercapacitor applications, Mater. Chem. Phys. 183 (2016) 571–579.
[37] M. Saranya, R. Ramachandran, F. Wang, Graphene-zinc oxide (G-ZnO) nanocomposite for electrochemical supercapacitor applications, Journal of Science: Advanced Materials and Devices 1 (4) (2016) 454–460.
[38] C.K. Maity, G. Hatui, K. Verma, G. Udayabhanu, D. Pathak, G.C. Nayak, Single pot fabrication of N doped reduced GO (N-rGO)/ZnO-CuO nanocomposite as an efficient electrode material for supercapacitor application, Vacuum 157 (2018) 145–154.
[39] L. Wang, H. Liu, J. Zhao, X. Zhang, C. Zhang, G. Zhang, Q. Liu, H. Duan, Enhancement of charge transport in porous carbon nanofiber networks via ZIF-8-enabled welding for flexible supercapacitors, Chem. Eng. J. (2019) 122979.
[40] Z. Xiong, C. Liao, W. Han, X. Wang, Mechanically tough large-area hierarchical porous graphene films for high-performance flexible supercapacitor applications, Adv. Mater. 27 (30) (2015) 4469–4475.
[41] J. Hao, X. Wang, F. Liu, S. Han, J. Lian, Q. Jiang, Facile synthesis ZnS/ZnO/Ni (OH) 2 composites grown on Ni foam: a bifunctional materials for photocatalysts and supercapacitors, Sci. Rep. 7 (1) (2017) 3021.
[42] B. Zeng, X. Chen, C. Chen, X. Ning, W. Deng, Reduced graphene oxides loaded-ZnS/CuS heteronanostructures as high-activity visible-light-driven photocatalysts, J. Alloys Compd. 582 (2014) 774–779.
[43] Y. Liang, N. Guo, L. Li, R. Li, G. Ji, S. Gan, Fabrication of porous 3D flower-like Ag/ZnO heterostructure composites with enhanced photocatalytic performance, Appl. Surf. Sci. 332 (2015) 32–39.
[44] L. Li, F. Tang, H. Liu, T. Liu, N. Hao, D. Chen, X. Teng, J. He, In vivo delivery of silica nanorattle encapsulated docetaxel for liver cancer therapy with low toxicity and high efficacy, ACS Nano 4 (11) (2010) 6874–6882.
[45] T. Liu, H. Liu, C. Fu, L. Li, D. Chen, Y. Zhang, F. Tang, Silica nanorattle with enhanced protein loading: a potential vaccine adjuvant, J. Colloid Interface Sci. 400 (2013) 168–174.
[46] D. Chen, L. Li, F. Tang, S. Qi, Facile and scalable synthesis of tailored silica "nanorattle" structures, Adv. Mater. 21 (37) (2009) 3804–3807.
[47] A. Van Blaaderen, J. Van Geest, A. Vrij, Monodisperse colloidal silica spheres from tetraalkoxysilanes: particle formation and growth mechanism, J. Colloid Interface Sci. 154 (2) (1992) 481–501.
[48] W. Stöber, A. Fink, E. Bohn, Controlled growth of monodisperse silica spheres in the micron size range, J. Colloid Interface Sci. 26 (1) (1968) 62–69.
[49] Y.-X. Wang, J. Yang, S.-L. Chou, H.K. Liu, W. Zhang, D. Zhao, S.X. Dou, Uniform yolk-shell iron sulfide–carbon nanospheres for superior sodium–iron sulfide batteries, Nat. Commun. 6 (2015) 8689.
[50] R. Shi, P. Yang, J. Wang, A. Zhang, Y. Zhu, Y. Cao, Q. Ma, Growth of flower-like ZnO via surfactant-free hydrothermal synthesis on ITO substrate at low temperature, CrystEngComm 14 (18) (2012) 5996–6003.
[51] Y. Sui, Y. Zhang, H. Hu, Q. Xu, F. Yang, Z. Li, High energy density asymmetric supercapacitor based ZnS/NiCo2S4/Co9S8 nanotube composites materials, Adv. Mater. Interfaces 5 (12) (2018), 1800018.
[52] R.S. Ganesh, G.K. Mani, R. Elayaraja, E. Durgadevi, M. Navaneethan, S. Ponnusamy, K. Tsuchiya, C. Muthamizhchelvan, Y. Hayakawa, ZnO hierarchical 3D-flower like architectures and their gas sensing properties at room temperature, Appl. Surf. Sci. 449 (2018) 314–321.

[53] H. Gong, N. Li, Y. Qian, Synthesis of SiO2/C nanocomposites and their electrochemical properties, Int. J. Electrochem. Sci. 8 (2013) 9811–9817.
[54] Z. Chen, W. Ren, L. Gao, B. Liu, S. Pei, H.-M. Cheng, Three-dimensional flexible and conductive interconnected graphene networks grown by chemical vapour deposition, Nat. Mater. 10 (6) (2011) 424.
[55] X. Dong, Y. Cao, J. Wang, M.B. Chan-Park, L. Wang, W. Huang, P. Chen, Hybrid structure of zinc oxide nanorods and three dimensional graphene foam for supercapacitor and electrochemical sensor applications, RSC Adv. 2 (10) (2012) 4364–4369.
[56] X. He, J.E. Yoo, M.H. Lee, J. Bae, Morphology engineering of ZnO nanostructures for high performance supercapacitors: enhanced electrochemistry of ZnO nanocones compared to ZnO nanowires, Nanotechnology 28 (24) (2017), 245402.
[57] Y.-L. Chen, Z.-A. Hu, Y.-Q. Chang, H.-W. Wang, Z.-Y. Zhang, Y.-Y. Yang, H.-Y. Wu, Zinc oxide/reduced graphene oxide composites and electrochemical capacitance enhanced by homogeneous incorporation of reduced graphene oxide sheets in zinc oxide matrix, J. Phys. Chem. C 115 (5) (2011) 2563–2571.
[58] A.J. Bard, L.R. Faulkner, J. Leddy, C.G. Zoski, Electrochemical Methods: Fundamentals and Applications, Wiley New, York, 1980.
[59] H. Pang, Y. Ma, G. Li, J. Chen, J. Zhang, H. Zheng, W. Du, Facile synthesis of porous ZnO–NiO composite micropolyhedrons and their application for high power supercapacitor electrode materials, Dalton Trans. 41 (43) (2012) 13284–13291.
[60] X. Xiao, B. Han, G. Chen, L. Wang, Y. Wang, Preparation and electrochemical performances of carbon sphere@ ZnO core-shell nanocomposites for supercapacitor applications, Sci. Rep. 7 (2017), 40167.
[61] Z. Li, P. Liu, G. Yun, K. Shi, X. Lv, K. Li, J. Xing, B. Yang, 3D (three-dimensional) sandwich-structured of ZnO (zinc oxide)/rGO (reduced graphene oxide)/ZnO for high performance supercapacitors, Energy 69 (2014) 266–271.
[62] J. Jayachandiran, J. Yesuraj, M. Arivanandhan, A. Raja, S.A. Suthanthiraraj, R. Jayavel, D. Nedumaran, Synthesis and electrochemical studies of rGO/ZnO nanocomposite for supercapacitor application, J. Inorg. Organomet. Polym. Mater. 28 (5) (2018) 2046–2055.
[63] A. Ramadoss, S.J. Kim, Facile preparation and electrochemical characterization of graphene/ZnO nanocomposite for supercapacitor applications, Mater. Chem. Phys. 140 (1) (2013) 405–411.
[64] P. Taberna, P. Simon, J.-F. Fauvarque, Electrochemical characteristics and impedance spectroscopy studies of carbon-carbon supercapacitors, J. Electrochem. Soc. 150 (3) (2003) A292–A300.
[65] P. Sivaraman, R. Kushwaha, K. Shashidhara, V. Hande, A. Thakur, A. Samui, M. Khandpekar, All solid supercapacitor based on polyaniline and crosslinked sulfonated poly [ether ether ketone], Electrochim. Acta 55 (7) (2010) 2451–2456.